Refereed Proceedings

The 12th International Conference on Fluidization - New Horizons in Fluidization Engineering

Engineering Conferences International *Year* 2007

Fluidized Bed Polymer Particle ALD Process for Producing HDPE/Alumina Nanocomposites

Joseph A. Spencer[*] Xinhua Liang[†] Steven M. George[‡]
Karen J. Buechler[**] John Blackson[††] Charles J. Wood[‡‡]
John R. Dorgan[§] Alan W. Weimer[¶]

[*]University of Colorado
[†]University of Colorado
[‡]University of Colorado
[**]University of Colorado
[††]Dow Chemical Company
[‡‡]Dow Chemical Company
[§]Colorado School of Mines
[¶]University of Colorado, alan.weimer@colorado.edu

FLUIDIZED BED POLYMER PARTICLE ALD™ PROCESS FOR PRODUCING HDPE/ALUMINA NANOCOMPOSITES

Joseph A. Spencer II[1], Xinhua Liang[1], David M. King[1], Steven M. George[1], Alan W. Weimer[1*], Karen J. Buechler[2], John Blackson[3], Charles J. Wood[3], and John R. Dorgan[4]

[1] Department of Chemical and Biological Engineering
University of Colorado, Boulder, CO 80309
[2] ALD NanoSolutions, Inc., Broomfield, CO 80020
[3] Dow Chemical Company, Midland, MI 48667
[4] Department of Chemical Engineering
Colorado School of Mines, Golden, CO 80401

*Corresponding author; E-mail: alan.weimer@colorado.edu

ABSTRACT

Micron-sized High Density Polyethylene (HDPE) particles were coated with ultrathin alumina (Al_2O_3) films in a Fluidized Bed Reactor (FBR) by Atomic Layer Deposition (ALD) at 77 ºC. Fluidization of HDPE particles were achieved at reduced pressure with the assistance of stirring or vibration. Al_2O_3 films on the HDPE particles were confirmed by different methods. These particles were extruded conventionally with the ceramic shells mixing intimately in the polymer matrix. The successful dispersion of the crushed Al_2O_3 shells in the polymer matrix following extrusion was confirmed.

INTRODUCTION

Polymeric materials can be greatly affected by nanoscopic inclusions of ceramic materials. These inclusions can result in increased impact, thermal stability, and flame resistance as well as decreased permeability (1,2). Prior work has primarily been done with nanoscopic montmorillonite clay (2-6). The inclusion of other ceramics has not been investigated to any extent.

Polymer/clay composites can be classified into three groups: conventional composites, intercalated nanocomposites, and exfoliated nanocomposites (4). A conventional composite is a simple mixture of clay aggregates and polymer. There is no fine dispersion or intimate mixing between the polymer and the clay, and they exist in segregated phases. Intercalated nanocomposites occur when clay hosts are intercalated with a few layers of polymer. These composites are typically over 50% clay and resemble the starting clay more than the added polymer. Exfoliated nanocomposites are nearly the opposite of an intercalated structure in that nanometer thick layers of clay are dispersed in a polymer matrix at much lower loading levels. These composites are more homogeneous than the conventional

The 12th International Conference on Fluidization - New Horizons in Fluidization Engineering, Art. 50 [2007]

composites or intercalated nanocomposites. The properties of the exfoliated nanocomposites reflect the starting polymer but are enhanced by the clay inclusions. Exfoliated nanocomposites are difficult to make, but provide the most impressive properties. One of the most recognized exfoliated structures is the combination of nylon-6 and montmorillonite discovered in the late 1980s by Toyota (5). The exfoliated nanocomposite demonstrated mechanical properties and thermal stability that were greatly improved over the base polymer material (6).

Problems are often encountered trying to achieve full exfoliation in polymer/clay nanocomposites. A novel process to promote intimate mixing is to coat polymer particles with ultrathin, uniform ceramic films by Particle ALD™ (ALD NanoSolutions, Inc., Broomfield, CO) in a Fluidized Bed Reactor (FBR). A FBR has the main advantages of good solid mixing, good heat transfer and ease of process control. The coated polymer particles can be extruded into pellets or films. Upon extrusion, the coated films are crushed, dispersing the shell remnants uniformly throughout the polymer matrix. The desired loading percent can be controlled by adjusting starting polymer particle size and the thickness of the ceramic films on the polymer particles. The incorporation of ceramic films directly onto the polymer particles prior to blending avoids complications experienced with conventional blending of dispersed nanoceramic materials into polymer matrices.

Atomic Layer Deposition (ALD) has a number of advantages over conventional deposition methods (7-10). Chemical Vapor Deposition (CVD) is one of the most prevalent surface coating techniques. However, CVD requires operating temperatures over 300°C, which is much higher than the melting point of the polymer. Plasma Enhanced CVD (PE-CVD) can aid in lowering the operating temperature (11,12), but this technique introduces high energy particles which can damage the polymer substrate. A sputtering technique may also be employed at an acceptable temperature, but it is a line-of-sight technique and cannot coat particles evenly or fill pores. ALD can solve all the above-mentioned problems.

Al_2O_3 ALD has been demonstrated on several substrates (13-16). Al_2O_3 is non-flammable and has a melting point of 2050 °C. In the realm of food packaging barrier film applications, Al_2O_3 is a good alternative to clay additives. Al_2O_3 provides a number of benefits over montmorillonite clay. HDPE is a widely used polymer and a good candidate for experimentation. Polyethylene and Al_2O_3 are also biocompatible. Combining these two materials could make a stronger polymer with many potential applications.

In this paper, the fluidization behavior of HDPE particles was studied, and a novel process to uniformly incorporate dispersed nanoceramic inclusions within a polymer matrix was demonstrated.

EXPERIMENTAL

The overall binary reaction for Al_2O_3 thin film growth is

$$2\ Al(CH_3)_3 + 3\ H_2O \rightarrow Al_2O_3 + 6\ CH_4 \quad (1)$$

This binary reaction can be divided into two half-reactions (8,9):

$$A)\ AlOH^* + Al(CH_3)_3 \rightarrow AlOAl(CH_3)_2^* + CH_4 \quad (2)$$

$$B)\ Al(CH_3)^* + H_2O \rightarrow AlOH^* + CH_4 \quad (3),$$

where * indicates a surface species. Each Al_2O_3 ALD half-reaction is self-limiting at temperatures as low as 33 ºC (13). The completion of each reaction provides the necessary functionalization to facilitate the subsequent reaction. When applied in an ABAB sequence, these reactions have been shown to deposit 1.25 Å Al_2O_3 per cycle at 77 ºC (13).

HDPE particles were obtained from Lyondell Chemical. They had an average size of 60 μm. The density of primary particles was 952 kg/m^3. The peak melting point was 135 ºC. The surface of HDPE particles was very rough, as shown in Figure 1. The HDPE particles were coated at 77°C at low pressure conditions using a FBR. A schematic of the experimental ALD-FBR is illustrated in Figure 2. The reactor was 6.35 cm in diameter in the fluidized bed area and 10.2 cm in diameter in the disengaging/filter area. Fluidization was assisted using a mechanical stirrer or two industrial vibration motors to vibrate the bed during fluidization. A porous metal disc with 20 μm pore size was used as the distributor plate. This ensured the exchange of surface contact points between particles and facilitated an even distribution of the precursors. The fluidized bed featured a disengaging zone which housed 4 porous metal filters that had the same porosity as the distributor plate.

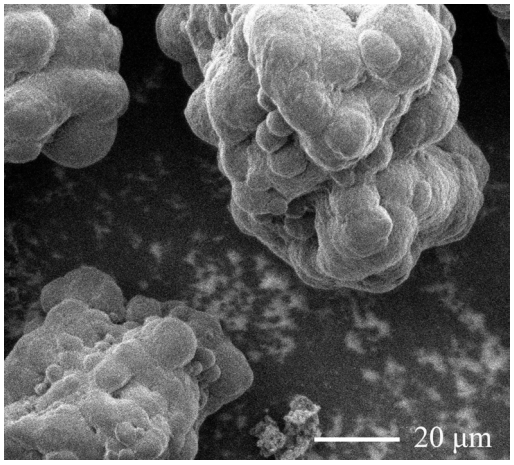

Figure 1. SEM of uncoated HDPE particles

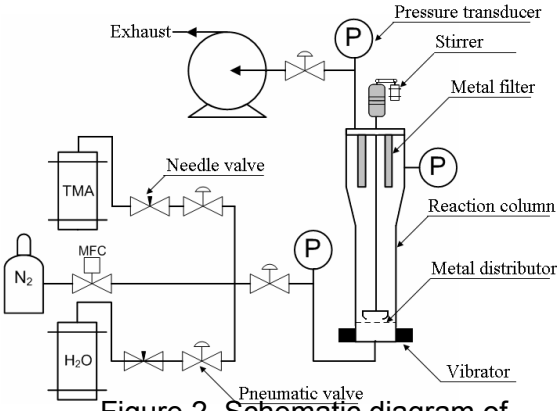

Figure 2. Schematic diagram of ALD-FBR system

The ALD reactions were carried out at pressures less than 400 Pa, as measured at the outlet of the FBR. For a typical experimental run, the reactor maintained a stable base line pressure of 85 Pa during N_2 purge flow of 0.35 cm/s. The bed consisted of 100 g of HDPE particles. During $Al(CH_3)_3$(TMA) doses, the TMA vapor was introduced into the N_2 carrier stream for 50 s, increasing the pressure of the reactor to approximately 160 Pa. The amount of TMA introduced into the FBR during the 50 s dose was equivalent to approximately 8×10^{-4} moles, which was approximately twice the stoichiometric amount necessary to saturate the TMA reaction. After the TMA reaction, the FBR was purged with N_2 for 70 s. The following 25 s H_2O dose resulted in a reactor pressure of approximately 240 Pa. The higher vapor pressure of H_2O allows for shorter dose times to achieve the same amount of exposure. Following the H_2O dose, the reactor was purged for 95 s. Subsequently, a 2 s blowback of N_2 flow was sent through the filters in the disengagement zone to remove any particles that may be collected on these filters. An additional purge of 50 s allowed for the reactor to return to its baseline pressure

The 12th International Conference on Fluidization - New Horizons in Fluidization Engineering, Art. 50 [2007]

before repeating the sequence. A small amount of N_2 gas always flowed through the bed to fluidize the particles.

To obtain different film thicknesses, batches of HDPE particles were exposed to 6, 13, 25, 50 and 100 TMA/H_2O cycles at 77 ºC. The HDPE particles subjected to 100 cycles were extruded in a custom, laboratory-sized (2.54 cm in diameter), Bonnot extruder at 175°C.

A Nicolet 750 Magna-IR Fourier Transform Infrared (FTIR) spectrometer was used to analyze the composition of the HDPE particles before and after coating. Inductively Coupled Plasma-Atomic Emission Spectroscopy (ICP-AES) was performed using an Applied Research Laboratories ICP-AES 3410+. Cross sectional Scanning Electron Microscopy (SEM) images were taken of Focused Ion Beam (FIB) milled coated polymer particles. The Particle Size Distribution (PSD) of HDPE particles before and after coating was determined using a particle size analyzer, Model 3225 Aerosizer from TSI. Surface area analysis was determined using a Quantachrome Autosorb-1. A Philips CM 10 Transmission Electron Microscope (TEM) was used to examine the dispersed shell remnants in the nanocomposite film.

RESULTS AND DISCUSSION

Fluidization Studies at Reduced Pressure Fluidization behavior of HDPE particles was investigated at reduced pressure and with stirrer and mechanical vibration applied to overcome some of the interparticle forces that were present. The fluidization experiments were carried out with the beginning pressure of about 10 Pa. To examine fluidization at low pressures, the pressure drop across the fluidized bed was recorded for a range of high purity N_2 gas flow rates. To obtain a baseline pressure profile, pressure drop values were obtained without particles in the reactor. These values were then subtracted from the pressure drop values obtained for the reactor with particles. This provided the pressure drop resulting from the particle bed alone. The pressure drop across the fluidized bed of particles reached a constant value at the minimum fluidization velocity. At this point, all of the polymer particles were being fluidized.

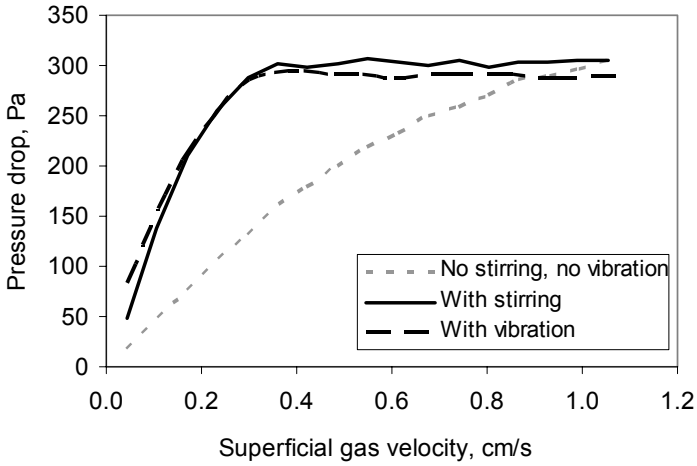

Figure 3. Fluidization curves for HDPE particles

The fluidization behavior of HDPE particles in the FBR is shown in Figure 3. Geldart Type C particles, such as micron-sized HDPE particles, are usually difficult to fluidize due to the highly cohesive nature of these particles (17). As shown in Figure 3, when no stirring or mechanical vibration was applied, pressure drop in the fluidized bed increased linearly with the superficial gas velocity and the gas flow may form channels through the particles. The particles were unable to achieve the separation

and true fluidization did not occur. With the assistance of stirring or mechanical vibration, fluidization was achieved and the minimum fluidization velocity occurred with 0.35 cm/s of N_2 flowing through the system. A stirrer and a mechanical vibrator showed the same effect to improve fluidization quality. This can be explain because vibration generates a pressure fluctuation that is transferred to the bed via a gas gap, which helps to partly overcome some interparticle forces (18); stirring can help to break aggregates of HDPE particles and reduce the formation of channels. This study shows that the fluidization of micron-sized HDPE particles can be achieved despite their high cohesive forces and the FBR system is suitable for ALD processing.

Al_2O_3 ALD on HDPE Particle Surface The surface of the HDPE particles was characterized by ex situ FTIR spectroscopy. As observed in Figure 4, the Al_2O_3 bulk infrared absorption mode is located at the frequency of 1100-500 cm^{-1}, and no Al_2O_3 signal appears for uncoated HDPE particles. An Al_2O_3 vibrational mode appears for coated particles after 50 and 100 cycles. This is a direct confirmation of the composition of the Al_2O_3 films on the polymer surface.

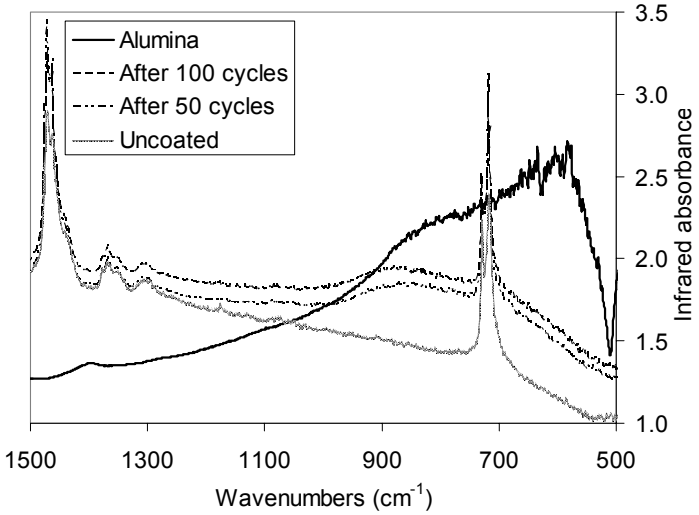

Figure 4. FTIR spectra of reference Al_2O_3, uncoated and Al_2O_3 coated HDPE particles after 50 and 100 cycles

ICP-AES analysis was performed on the various batches to determine their aluminum concentrations. In general, the aluminum concentration increased with the number of coating cycles. A previous study used a Quartz Crystal Microbalance (QCM) to monitor the mass increase during Al_2O_3 ALD on spin-coated polyethylene (19). The ICP-AES data from this study and the QCM data from the previous study are plotted versus the number of coating cycles in Figure 5. Both sets of data display the same qualitative trends. The lower initial growth rate of Al_2O_3 shows that there was a delay before film growth started. This nucleation regime consists of approximately 15 cycles. Similar nucleation periods were observed during Al_2O_3 ALD on various other spin-coated polymer films including polyethylene (19).

The Al_2O_3 ALD is conventionally thought to begin with native hydroxyl groups on the surface. HDPE, however, is one kind of polymer that has no native hydroxyl groups. So, the fundamental concept of Al_2O_3 ALD cannot take place on the HDPE particle surface. This nucleation behavior has been attributed to the absorption of TMA followed by its subsequent reaction with H_2O to create Al_2O_3 clusters in the near-surface regions of the polymer. HDPE has a porous surface, and both HDPE and TMA are nonpolar, so it is expected that TMA has a reasonable solubility in the HDPE particle, and TMA can adsorb onto the surface of the polymer and subsequently diffuse into the near-surface regions of the polymer (14,19). Therefore,

The 12th International Conference on Fluidization - New Horizons in Fluidization Engineering, Art. 50 [2007]

during the ALD reaction, the incoming H_2O will react efficiently with TMA molecules at or near the surface of the polymer particle and Al_2O_3 clusters will be formed. After several coating cycles, the Al_2O_3 clusters will eventually merge to create a continuous adhesion layer on the polymer particle surface (14,19). Al_2O_3 clusters with hydroxyl groups will provide a "foothold" for the deposition of Al_2O_3 films on the polymer. In Figure 5, the highest growth rate is observed at cycles of 40-50. This behavior is explained by the fact that after the nucleation period, the Al_2O_3 clusters become larger and eventually seal off the surface of the polymer with a roughened, continuous Al_2O_3 film. The higher surface area of the roughened Al_2O_3 film can lead to a slightly enhanced growth rate immediately following the nucleation period. Further deposition has a smoothing effect on the Al_2O_3 film and the growth rate decreases to approach a normal value.

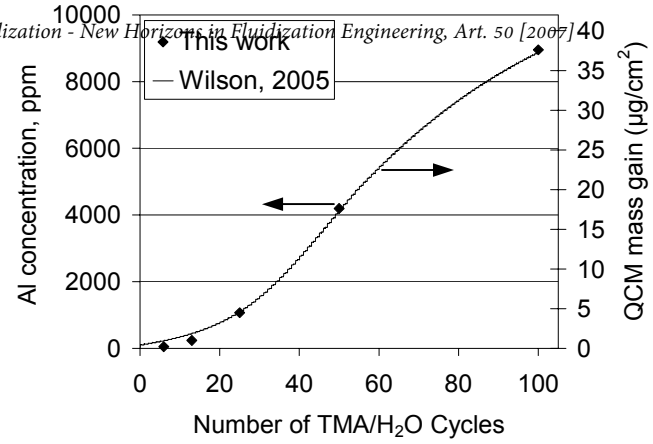

Figure 5. ICP-AES mass gain vs. in situ growth comparison

Focused Ion Beam (FIB) cross sectional SEM image allows precise observation at the edge interface of the polymer and Al_2O_3 film. The SEM image of HDPE particles exposed to 100 cycles at 77°C is shown in Figure 6. Islands mirroring the theoretical growth mechanism can be observed. Islanding begins below the surface and the film merges into a linear layer as it grows. The SEM image shows that the Al_2O_3 films appear to be very uniform and smooth. Approximately 35±7 nm thick Al_2O_3 films were coated on the polymer surface. This thickness represents a growth rate of about 0.4 nm per coating cycle at this experimental condition.

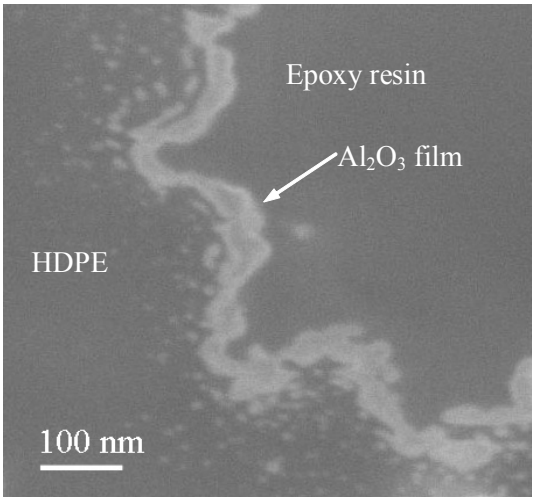

Figure 6. FIB cross sectional SEM of Al_2O_3 coated HDPE particle

The Al_2O_3 film growth rate was much higher than the 0.11~0.13 nm per cycle of an ALD process reported in the literature (10,13). Recent FTIR measurements of Al_2O_3 ALD on Low Density Polyethylene (LDPE) indicated the presence of hydrogen-bonded H_2O molecules on the Al_2O_3 surface (14). This higher growth rate may be explained by the presence of hydrogen-bonded H_2O. This H_2O can react with TMA to deposit additional Al_2O_3 by CVD (14). Another reason is the increase in the surface coverages of reactants at the lower temperatures (13). Though the reaction kinetics is slower at lower temperatures, the growth rate is determined by the higher surface coverages.

Fine particles will aggregate during fluidization because of interparticle forces, such as Van de Waals forces (16). The PSD curves for uncoated HDPE particles and 50 cycles HDPE particles are shown in Figure 7. As shown in the plot, the size of particles remains fairly unchanged after the coating process, meaning that no aggregates were being coated. This is also evident from the results of BET surface area before coating (0.24 m^2/g) and after coating (0.28 m^2/g), which indicates that the individual particles were coated as opposed to necking multiple particles during the reaction (16).

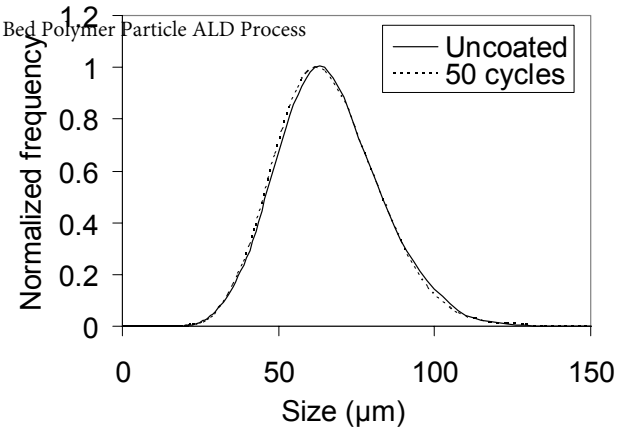

Figure 7. PSD of uncoated and Al_2O_3 coated HDPE particles

HDPE/Al_2O_3 Nanocomposite The Al_2O_3 coated HDPE particles after 100 cycles were successfully extruded into HDPE/Al_2O_3 nanocomposite pellets. The extruded pellets were cut using a microtome to achieve a thickness of approximately 100 nm for TEM analysis. A cross sectional TEM image of the nanocomposite is shown in Figure 8. Image (a) shows a scattering of nanosized inclusions of Al_2O_3 flakes throughout the sample. Hence, a uniformly dispersed nanocomposite was formed. The large diagonal features are small peels in the cross section resulting from the blade of the microtome skipping across the polymer. This skipping did not affect the imaging. Looking at one of the Al_2O_3 flakes in image (a) at higher magnification, image (b) demonstrates that the Al_2O_3 flakes were formed of much smaller Al_2O_3 particles.

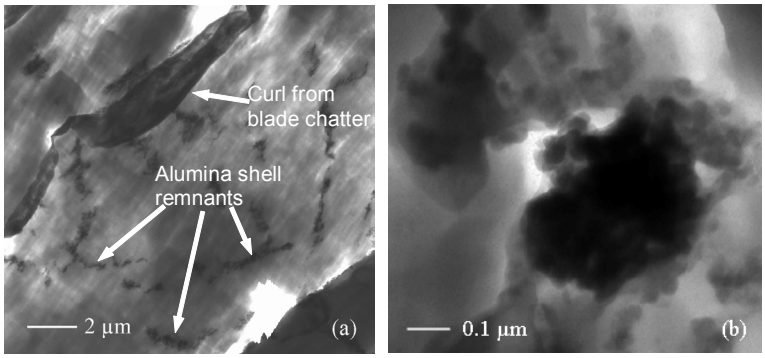

Figure 8. Cross sectional TEM of HDPE/Al_2O_3 nanocomposite film

CONCLUSIONS

Incorporating a low weight percent of well dispersed nano-ceramic material by a novel fluidized bed polymer Particle ALD™ process was demonstrated. Fluidization of micron-sized HDPE particles were achieved at reduced pressure with the assistance of stirring or vibration. Particle ALD™ was used successfully to deposit a thin film of Al_2O_3 on the surface of individual HDPE particles. Successful Al_2O_3 coating on the HDPE particles was confirmed using FTIR, ICP-AES and cross sectional SEM. A nucleation mechanism for Al_2O_3 ALD at the polymer surface was confirmed. The results of PSD and surface area of the uncoated and the nanocoated particles showed that there was no aggregation of nanocoated particles during the coating process. The coated HDPE particles were then extruded to crush the Al_2O_3

shells. Cross sectional TEM indicated that nanoscale crushed Al_2O_3 shells were successfully dispersed in the polymer matrix.

ACKNOWLEDGEMENTS

This work was supported by NSF grant 0400292. The authors thank Lyondell Chemical for providing the HDPE particles. The authors also thank Fredrick G. Luiszer at the University of Colorado for providing the ICP-AES analysis as well as Thomas H. Giddings at the University of Colorado for assistance with the TEM work.

REFERENCES

1. Messersmith, P. B., and Giannelis, E. P., *Journal of Polymer Science Part A-Polymer Chemistry*, 1995, **33**(7): 1047-1057.
2. Maiti, P., Yamada, K., Okamoto, M., Ueda, K., and Okamoto, K., *Chemistry of Materials*, 2002, **14**(11): 4654-4661.
3. Kojima, Y., Usuki, A., Kawasumi, M., Okada, A., Kurauchi, T., Kamigaito, O., and Kaji, K., *Journal of Polymer Science Part B-Polymer Physics*, 1994, **32**(4): 625-630.
4. Lan, T., Kaviratna, P. D., and Pinnavaia, T. J., *Chemistry of Materials*, 1994, **6**(5): 573-575.
5. Fukushima, Y., and Inagaki S., *Journal of Inclusion Phenomena*, 1987, **5**(4): 473-482.
6. Usuki, A., Kojima, Y., Kawasumi, M., Okada, A., Fukushima, Y., Kurauchi, T., and Kamigaito, O., *Journal of Materials Research*, 1993, **8**(5): 1179-1184.
7. Suntola, T., *Thin Solid Films*, 1992, **216**(1): 84-89.
8. George, S. M., Ott, A. W., and Klaus, J. W., *Journal of Physical Chemistry*, 1996, **100**(31): 13121-13131.
9. Dillon, A. C., Ott, A. W., Way, J. D., and George, S. M., *Surface Science*, 1995, **322**(1-3): 230-242.
10. Ott, A. W., Klaus, J. W., Johnson, J. M., and George, S. M., *Thin Solid Films*, 1997, **292**(1-2): 135-144.
11. Sobrinho, A. S. D., Czeremuszkin, G., Latrèche, M., Dennler, G., and Wertheimer, M. R., *Surface & Coatings Technology*, 1999, **119**: 1204-1210.
12. Sobrinho, A. S. D., Czeremuszkin, G., Latrèche, M., and Wertheimer, M. R., *Journal of Vacuum Science & Technology A*, 2000, **18**(1): 149-157.
13. Groner, M. D., Fabreguette, F. H., Elam, J. W., and George, S. M., *Chemistry of Materials*, 2004, **16**(4): 639-645.
14. Ferguson, J. D., Weimer, A. W., and George, S. M., *Chemistry of Materials*, 2004, **16**(26): 5602-5609.
15. Hakim, L. F., Blackson, J., George, S. M., and Weimer, A. W., *Chemical Vapor Deposition*, 2005, **11**(10): 420-425.
16. Wank, J. R., George, S. M., and Weimer, A. W., *Powder Technology*, 2004, **142**(1): 59-69.
17. Geldart, D., *Powder Technology*, 1973, **7**(5): 285-292.
18. Hakim, L. F., Portman, J. L., Casper, M.D., and Weimer, A. W., *Powder Technology*, 2005, **160**(3): 149-160.
19. Wilson, C. A., Grubbs, R. K., and George, S. M., *Chemistry of Materials*, 2005, **17**(23): 5625-5634.